Materials Advances

ROYAL SOCIETY OF CHEMISTRY

PAPER

View Article Online
View Journal | View Issue

Cite this: *Mater. Adv.*, 2025, **6**, 7436

Modification of electron acceptors with fused alicyclic rings through inverse electron-demand Diels–Alder reactions to tune the optical properties of conjugated polymers

Dinghui Chen,†[ac] Kang Le Osmund Chin,†[b] Xiang Yun Debbie Soo,[c] Feng Xia Wei,[c] Ke Li,[c] Pin Jin Ong,[c] Qiang Zhu,[c] Xizu Wang,[c] Teck Lip Dexter Tam,[c] Zhuang Mao Png,[b] Ming Hui Chua,[b] Hong Meng*[d] and Jianwei Xu*[be]

Received 17th May 2025,
Accepted 22nd August 2025

DOI: 10.1039/d5ma00507h

rsc.li/materials-advances

Traditional strategies for manipulating the optical properties of conjugated polymers primarily focus on modifications of the polymer backbone, including donor–acceptor engineering and adjusting the conjugation length. Here, we report a novel approach to modulate the electronic structure of conjugated polymers by incorporating alicyclic rings through inverse electron-demand Diels–Alder reactions. Two conjugated polymers, **PCT-8** and **PBT-7**, were synthesized using monomers with an eight-membered and a bridged six-membered aliphatic ring, respectively. These structural modifications lead to noticeable changes in UV-visible absorption ($\Delta\lambda_{max}$ = 47 nm for **PCT-8** and **PBT-7**), optical band gaps (2.38 eV and 2.19 eV, **PCT-8** and **PBT-7**, respectively), polymer packing, and intermolecular interactions, while maintaining the integrity of the polymer backbone. Besides, both polymers demonstrate electrochromic properties. This strategy offers a versatile, minimally invasive method for tuning the optical properties of conjugated polymers, paving the way for the design of multifunctional materials for optoelectronic applications.

1. Introduction

Electron-deficient π-conjugated units, referred to as electron acceptors, are essential components in the design and synthesis of functional organic electronic materials.[1] Electron acceptors play a pivotal role in tuning the energy levels of the frontier orbitals and modulating the optical properties of the materials.[2,3] In numerous instances, the selection of an appropriate electron acceptor is a crucial factor that influences the performance of the resulting materials. One of the defining characteristics of electron acceptors is their significant electron deficiency, which is critical for a wide range of applications, such as donor–acceptor dyes with near-infrared absorption and emission,[4] n-type organic thermoelectric materials,[5] electrochromic materials[6–9] and light-harvesting components in organic light-emitting diodes.[10]

In our previous work, we introduced electron-deficient π-conjugated units by using Diels–Alder reactions. For example, we reported the synthesis of a highly electron-deficient acceptor, pyrrolopyridazinedione (PPD), characterized by ultra-high electron deficiency.[1] PPD-thiophene was copolymerized with 3,4-propylenedioxythiophene to obtain three polymers: **P1**, **P2**, and **P3** (Table S1, SI). Additionally, we developed a novel electron acceptor, pyrrolo-acenaphtho-pyridazinedione (PAPD), that exhibits ultra-high electron deficiency for the synthesis of donor–acceptor conjugated polymers. The PAPD monomers, which have a low LUMO energy level of −3.42 eV, were synthesized through a regioselective inverse electron demand Diels–Alder reaction, obtaining a series of high-molecular-weight electrochromic polymers (**P4–P8**) (Table S1, SI). These polymers exhibit absorption maxima of about 500–530 nm, as well as reversible color transitions from purple/red to greyish blue/grey.[11] Recently, we explored the use of fluorinated

[a] *Frontiers Science Center for Flexible Electronics (FSCFE) & Institute of Flexible Electronics (IFE), Northwestern Polytechnical University (NPU), 127 West Youyi Road, Xi'an 710072, China*
[b] *Institute of Sustainability for Chemicals, Energy and Environment (ISCE2), Agency for Science, Technology and Research (A*STAR), Singapore, 1 Pesek Road, Jurong Island, Singapore 627833. E-mail: Xu_Jianwei@isce2.a-star.edu.sg*
[c] *Institute of Materials Research and Engineering (IMRE), Agency for Science, Technology and Research (A*STAR), Singapore, 2 Fusionopolis Way, Innovis, #08-03, Singapore 138634*
[d] *School of Advanced Materials, Peking University Shenzhen Graduate School, Peking University, Shenzhen, 518055, China. E-mail: menghong@pku.edu.cn*
[e] *Department of Chemistry, National University of Singapore (NUS), Singapore, 3 Science Drive 3, Singapore 117543*
† Both are equally contributed to the paper.

electron acceptors synthesized *via* the inverse electron demand Diels–Alder reaction involving tetrazine with 1-ethynyl-4-fluorobenzene and 1-allyl-2,3,4,5,6-pentafluorobenzene.[8] Three new electron acceptors were polymerized with 5,5-ditin-bithiophene to form conjugated polymers, exhibiting solution-state absorption maxima ranging from approximately 465 nm to 485 nm.

In earlier research, the primary focus was on the electronic properties of the donor acceptor pair. However, the tunability of the polymer was somewhat limited, with a difference in absorption maxima of only up to 30 nm despite a significant difference in the electronic properties. In the current study, we introduce an approach by incorporating two diverse types of alicyclic rings as substituents: an eight-membered aliphatic ring and a six-membered ring with a CH_2 bridge. These were polymerized with thiophene-based monomers to yield two new conjugated polymers, **PCT-8** and **PBT-7**. Although both polymers exhibited aliphatic pendent groups with presumably similar electronic properties, they exhibited a surprising difference in the optical properties, with an absorption maxima difference of 47 nm.

We postulate that this discrepancy arises from the difference in the spatial arrangement of the substituents, affecting their HOMO, LUMO, and bandgap characteristics. This finding provides a complementary strategy for tuning the properties of conjugated polymers together with conventional methods such as the donor–acceptor strategy,[12–19] adjusting the conjugation length,[20–22] heteroatom doping,[20–22] and π–π stacking[23,24] to modulate the bandgap of conjugated polymers. The results highlight the potential of the unique structure of an aliphatic ring to be used as a powerful tool for tailoring the optoelectronic properties of conjugated polymers, paving the way for developing innovative strategies for designing conjugated polymers.

2. Experimental section

2.1. Measurements

Nuclear magnetic resonance (NMR) spectra were recorded on a JEOL ECA-II 400 or 500 MHz NMR instrument using $CDCl_3$ as the solvent. UV-vis and UV-vis-NIR absorption spectra were recorded with a Shimadzu UV-3600 UV-vis-NIR spectrophotometer. Cyclic voltammetry (CV) was carried out using an Auto lab PGSTAT128N potentiostat. The measurements were conducted in a glove box in a three-electrode cell configuration, with the polymer-coated glassy carbon as the working electrode, Pt wire as the counter electrode, and Ag wire as the pseudo-reference electrode. The electrolyte/solvent couple used was 0.1 M $LiClO_4$ in acetonitrile, with measurements taken at a scan rate of 50 mV s^{-1}. *In situ* electrochromic studies were performed using both the potentiostat and spectrophotometer. The atomic force microscopy (AFM) images were obtained using the Bruker Dimension Icon SPM, and a high-resolution scanning probe microscope was used for detailed surface characterization and imaging. X-ray diffraction (XRD) patterns of the thin films were recorded in reflection mode using Cu-K_α radiation (λ = 0.15406 nm) on a Bruker D8 General Area Detector Diffraction System. Photoluminescence measurements were performed using a HORIBA Jobin Yvon Fluorolog® spectrofluorometer. Thermogravimetric analysis (TGA) was conducted on a TGA Q500 from TA Instruments. The differential scanning calorimetry (DSC) testing was carried out using Q100, TA Instruments, USA.

2.2. Material synthesis

The monomers, 1,4-bis(5-bromothiophen-2-yl)-5,6,7,8,9,10-hexahydrocycloocta[*d*]pyridazine (**M4**) and 1,4-bis(5-bromothiophen-2-yl)-5,6,7,8-tetrahydro-5,8-methanophthalazine (**M5**), were synthesized through an inverse electron-demand Diels–Alder reaction between 3,6-bis(5-bromothiophen-2-yl)-1,2,4,5-tetrazine and (*Z*)-cyclooctene and bicyclo[2.2.1]hept-2-ene, obtaining 67% and 25%, respectively. Next, these monomers were subjected to Stille cross-coupling polymerization with the compound **6**, (4,4′-didodecyl-[2,2′-bithiophene]-5,5′-diyl)bis(trimethylstannane), resulting in the formation of polymers **PCT-8** and **PBT-7**, respectively.

2.3. Fabrication of devices

The polymer solution (10 mg mL^{-1}, in a 1 : 1 (V/V) mixture of chloroform and chlorobenzene) was filtered and spin-coated onto ITO substrates at 1000 rpm for 30 seconds to yield a film thickness of around 30 nm. Excessive polymer edges were removed by swabbing with chloroform using a cotton bud to obtain an active area of 2 × 2 cm^2. On another piece of the ITO substrate, a 2 × 2 cm^2 area was blocked out using a parafilm spacer. 275 μL of the gel electrolyte (prepared by dissolving 0.512 g of lithium perchlorate and 2.8 g of poly(methyl methacrylate) (molecular weight = 120 000 g mol^{-1}) in 6.65 mL of propylene carbonate) and 28 mL of dry acetonitrile were pipetted into the 2 × 2 cm^2 area and left to dry for 15 minutes. The device was fabricated by assembling the two ITO glass

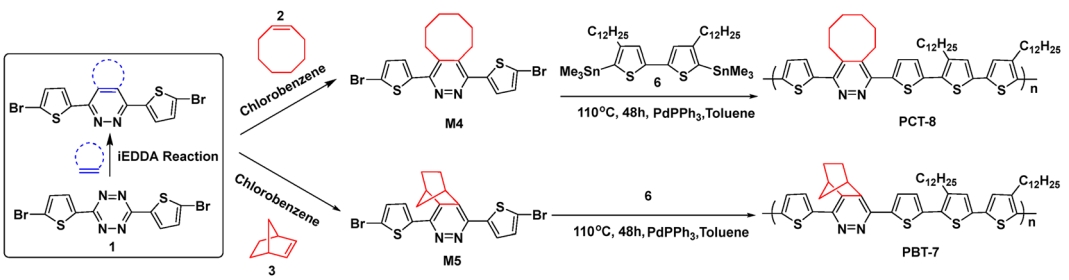

Fig. 1 Synthetic routes leading to polymers **PCT-8** and **PBT-7**.

substrates together with the polymer film and the gel electrolyte in contact.

3. Results and discussion

3.1. Synthesis of polymers

The synthesis route leading to the two polymers, **PCT-8** and **PBT-7**, is illustrated in Fig. 1. First, compound **1** was reacted with (*Z*)-cyclooctene and bicyclo[2.2.1]hept-2-ene to produce the monomers **M4** and **M5**, with yields of 25 and 67%, respectively. The low yield of **M4** is likely due to side reactions of highly strained bicyclo[2.2.1]hept-2-ene, particularly at high temperatures. These two monomers were subsequently reacted with compound **6**, (4,4′-didodecyl-[2,2′-bithiophene]-5,5′-diyl)bis(trimethylstannane), to yield the respective polymers **PCT-8** and **PBT-7**. The polymers were purified *via* Soxhlet extraction, resulting in solid products with yields of 76% for PCT-8 and 69% for PBT-7. The molecular weights and polydispersity indices of the two polymers were determined using gel permeation chromatography, with the results summarized in Table 1 (below).

3.2. Optical and electrochemical properties

As shown in Fig. 2, **PCT-8** and **PBT-7** exhibit distinct optical behaviors. In solution, **PCT-8** shows a maximum absorption at 435 nm (red), while **PBT-7** absorbs at 388 nm (yellow). The 47 nm bathochromic shift of **PCT-8** implies that it has better intramolecular conjugation than **PBT-7**. Upon transitioning to the solid-state thin film, the absorption peaks of both polymers undergo further red-shifts, with the peak of **PCT-8** shifting to 451 nm and the peak of **PBT-7** moving to 400 nm. This red-shift observed in the solid state, compared to the solution state, indicates enhanced π–π stacking interactions. These stronger π–π interactions deepen the conjugation and boost intermolecular forces, leading to improved optoelectronic properties in the polymers. In contrast to **PCT-8** and the above-mentioned polymers (Table S1), different absorption characteristics of **PBT-7** may be due to its steric hindrance effect.

The HOMO and LUMO energy levels of the two polymers were determined using cyclic voltammetry. Fig. S1 presents the cyclic voltammograms of the polymer thin films, where two polymers exhibit quasi-reversible oxidation and reduction behavior.

The cyclic voltammogram (CV) of ferrocene is shown in Fig. S2. As presented in Table 1, the HOMO energy levels for the polymers **PCT-8** and **PBT-7** were estimated to be −5.14 eV and −5.54 eV, respectively, with corresponding LUMO levels of 2.76 eV for **PCT-8** and 3.35 eV for **PBT-7**. The bandgap (E_g) values were calculated as 1.93 eV for **PCT-8** and 1.66 eV for **PBT-7**. **PCT-8** exhibits a lower bandgap than **PBT-7**, which correlates with their observed colors. **PCT-8** appears red, while **PBT-7** appears yellow. The optical band gaps, estimated from the onset absorption wavelengths of thin-film polymers, tend to be larger than those obtained from the CV method. This discrepancy is likely because optical measurements such as UV-Vis spectroscopy measure the energy required for an electron to transition to the first excited state.

Additionally, density functional theory (DFT) calculations were performed on the oligomers **PCT-8** and **PBT-7**. As shown in Fig. S3, the simplified molecular models of these conjugated polymers, together with their HOMO and LUMO distributions and corresponding energy levels, are displayed. The HOMO and LUMO energy levels for **PCT-8** are −4.81 eV and −2.23 eV, respectively, while for **PBT-7** they are −4.76 eV and −2.30 eV. Their corresponding band gaps for **PCT-8** and **PBT-7** are 2.58 eV and 2.46 eV, which are close to their optical band gaps of 2.38 eV and 2.19 eV, respectively. The HOMO and LUMO electron density distributions reveal that the π-electron clouds are predominantly localized on the conjugated units along the polymer backbone, indicating effective electron delocalization. The differences observed between the experimentally determined and DFT-calculated HOMO and LUMO levels are attributed to the use of simplified oligomer models in the DFT calculations, which omit the side chains to reduce computational complexity.

To explore the influence of structural differences on the optical properties, we conducted single-crystal structural analyses of monomer **4** (**M4**) and monomer **5** (**M5**). As shown in Fig. 3, **M4** and **M5** exhibit distinct molecular structures. The single-crystal structure data are summarized in Table S2. For **M4**, the dihedral angles between the thiophene and tetrazine units are 14.90° (left) and 15.07° (right). In contrast, the corresponding dihedral angles between the thiophene and tetrazine units for **M5** are 19.29° (left) and 11.97°(right). In addition, the average dihedral angle between the thiophene and tetrazine units is 14.99° for **M4**, while the average dihedral angle between the thiophene and tetrazine units is 15.63° for **M5**.

Generally, large dihedral angles weaken π-orbital overlap, thereby compromising the overall conjugation within the polymer and leading to a wider electronic bandgap. Compared to the bridged six-membered ring in **M5**, the eight-membered ring in monomer **M4** imposes less steric hindrance. As a result, the steric hindrance in polymer **PCT-8** is relatively low, whereas **PBT-7** suffers from greater steric hindrance, which disrupts its

Table 1 Molecular weights, PDI and synthesis yields of polymers

Polymers	$\lambda_{max,solution}$ (nm)	$\lambda_{max,flim}$ (nm)	$\lambda_{onset,flim}$ (nm)	$E_g^{opt\,a}$ (eV)	$E_{HOMO}{}^{b}$ (eV)	$E_{LUMO}{}^{c}$ (eV)	$E_g{}^{d}$ (eV)	$M_n{}^{e}$ (kDa)	$M_w{}^{f}$ (kDa)	PDI[g]	Synthesis yields
PCT-8	435	451	521	2.38	−5.14	−2.76	1.93	10	17	1.64	76%
PBT-7	388	400	565	2.19	−5.54	−3.35	1.66	7.2	11	1.58	69%

[a] $E_g = \frac{1240}{\lambda_{onset}}$ (1). [b] $E_{HOMO} = -(E_{onset,ox} + 4.8)$ (2). [c] $E_{LUMO} = -(E_{onset,red} + 4.8)$ (3). [d] $E_g = E_{LUMO} - E_{HOMO}$. [e] M_n: number-average molecular weight. [f] M_w: weight average molecular weight. [g] PDI: polydispersity index.

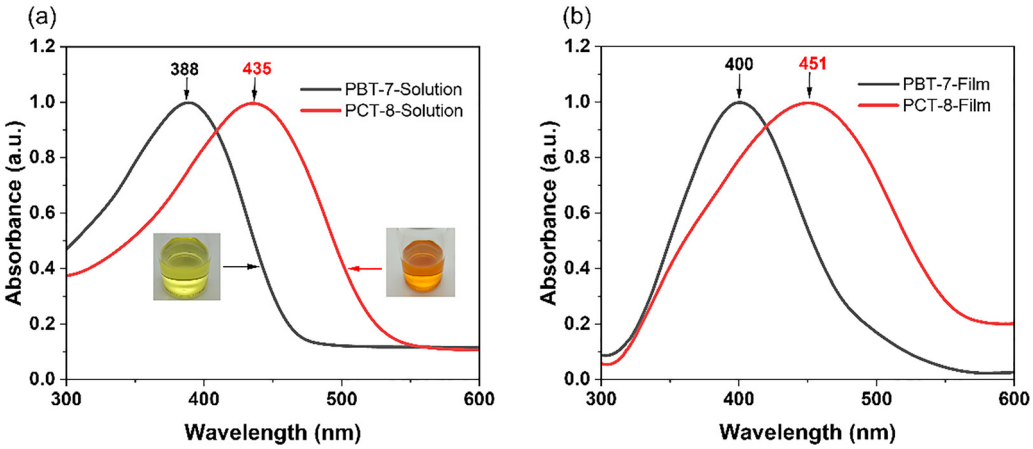

Fig. 2 (a) Normalized UV-Vis absorption spectra of **PCT-8** and **PBT-7** in chloroform solution with the corresponding photographs of the solutions; (b) normalized UV-vis absorption spectra of **PCT-8** and **PBT-7** in thin films and the corresponding photographs.

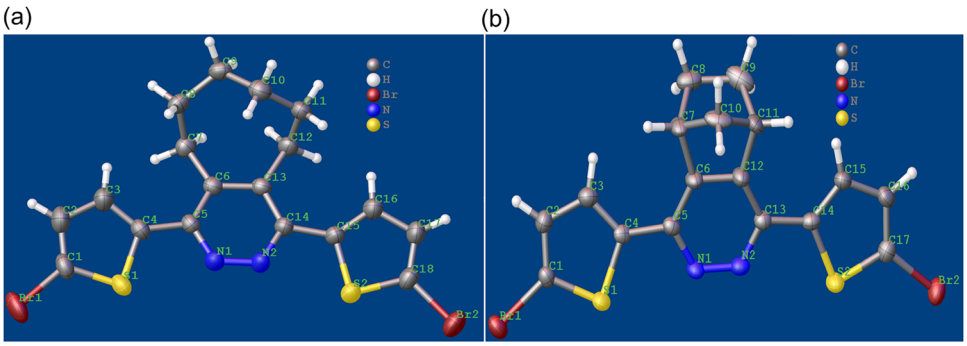

Fig. 3 (a) Single crystal of monomer **M4**; (b) single crystal of monomer **M5**.

π-conjugation. Consequently, **PBT-7** exhibits a blue-shifted maximum absorption wavelength (λ_{max}) at 388 nm in chloroform, while the enhanced conjugation in **PCT-8** results in a red-shifted λ_{max} at 435 nm.

M5 exhibits a maximum dihedral angle of 19.29°, significantly larger than that of **M4**. This larger dihedral angle reduces π-conjugation efficiency in **M5**, resulting in a wider electronic bandgap, a blue shift in the absorption spectrum to 388 nm. In contrast, the smaller dihedral angles in **M4** enhance π-conjugation efficiency, leading to a red shift in its absorption spectrum to 435 nm. Additionally, as shown in Table S2, according to the bond length data, the N= and N–C bonds in **M5** are slightly longer than those in **M4**, which may weaken the π-orbital overlap efficiency and further reduce the overall conjugation. In contrast, the better conjugation in **M4** leads to a red shift in the absorption spectrum of its corresponding polymer **PCT-8**, whereas the poorer conjugation in **M5** results in a blue shift in **PBT-7**. This trend in the optical properties is consistent with their molecular structural differences.

To further investigate the thermal properties of the polymers, DSC and TGA measurements were conducted. TGA measurements were carried out under a nitrogen atmosphere with a heating rate of 10 °C min^{-1}. As shown in Fig. S4, both polymers exhibit good thermal stability, with 5% weight loss temperatures (T_d^5%) of approximately 304 °C for **PCT-8** and 263 °C for **PBT-7**. After 900 °C, both polymers exhibit a negligible residual carbon content. The slightly higher thermal decomposition temperature and residual weight of **PCT-8** indicate enhanced thermal stability. For DSC analysis, no obvious glass transition temperature (T_g) was observed within the measured range of 30–200 °C. The absence of a clear T_g may result from the rigid conjugated backbone, which restricts chain mobility and leads to a higher or undetectable T_g within the measured range. Moreover, no significant melting peak was observed, indicating that both polymers are largely amorphous. This amorphous nature helps ensure uniform film formation and better morphological stability in optoelectronic applications.

To investigate the morphological characteristics of the two polymer films, atomic force microscopy (AFM) analysis was performed. Fig. S5 presents AFM images of two polymer films. In Fig. S5a, the average surface roughness (R_a) of the polymer **PCT-8** film is measured to be 0.39 nm, indicating a relatively smooth and uniform surface. In contrast, Fig. S5b shows the polymer **PBT-7** film with a significantly rougher surface, exhibiting a R_a of 1.01 nm. In contrast, the surface in Fig. S5b exhibits pronounced fibril-like structures and interconnected

networks, suggesting higher surface roughness. This enhanced texture could result from polymer aggregation, phase separation, or crystalline domains within the film. The differences in the morphology between the two films may significantly influence their properties in the solid state. To investigate the differences in crystallinity between the two polymer films, X-ray diffraction (XRD) analysis was conducted. As shown in Fig. S6, both **PCT-8** and **PBT-7** exhibit broad diffraction peaks, indicating their predominantly amorphous nature. However, **PBT-7** shows significantly higher diffraction intensity than **PCT-8**, particularly at $2\theta \approx 10^{\circ}$ and 25°, suggesting a greater degree of molecular ordering or localized crystallinity. This disparity likely arises from differences in their chemical structures and intermolecular interactions. The higher crystallinity of **PBT-7** can be attributed to its enhanced π–π stacking interactions, facilitated by its segmental structure, whereas the structural characteristics of **PCT-8** may result in a more loosely packed molecular arrangement. These variations in molecular packing and crystallinity may play a crucial role in determining the distinct absorption behaviors of the two polymers. In general, in an electrofluorochromic device, crystallinity can be optimized to balance charge transport and excitation confinement, while an ultra-smooth interface (*e.g.*, less than a few nanometers RMS roughness) can significantly enhance fluorescence output. In our case, the roughness, not exceeding 1.1 nm, together with the amorphous nature of the two polymers **PBT-7** and **PCT-8**, suggest a limited influence on device parameters. The observed differences are primarily attributed to the polymer structures, which induce variations in their optical and physical properties.

3.3. Performance of electrochromic and fluorescent dual-function devices

Fig. 4a and b display the electrochromic behavior of devices with **PCT-8** and **PBT-7** as the electrochromic layers, respectively, highlighting their optical transitions between neutral and colored states. Spectroelectrochemistry studies showed that while **PBT-7** revealed an overall broad increase in absorption from *ca.* 500 to 1600 nm as the applied positive voltages increased, **PCT-7** revealed the evolution of a small absorption band at *ca.* λ_{abs} of 720 nm, along with a broad increase in absorption beyond *ca.* 1000 nm. This was accompanied by an intensified increase in absorption in the UV range. These changes are reflected by **PCT-8** undergoing a colour change from reddish orange to cyan whereas **PBT-7** underwent a pale yellow to blue-cyan colour change (Fig. 4a and b). Further kinetic studies on **PCT-8** switching at ± 2.0 V monitored through the transmittance at 456 nm showed that the device

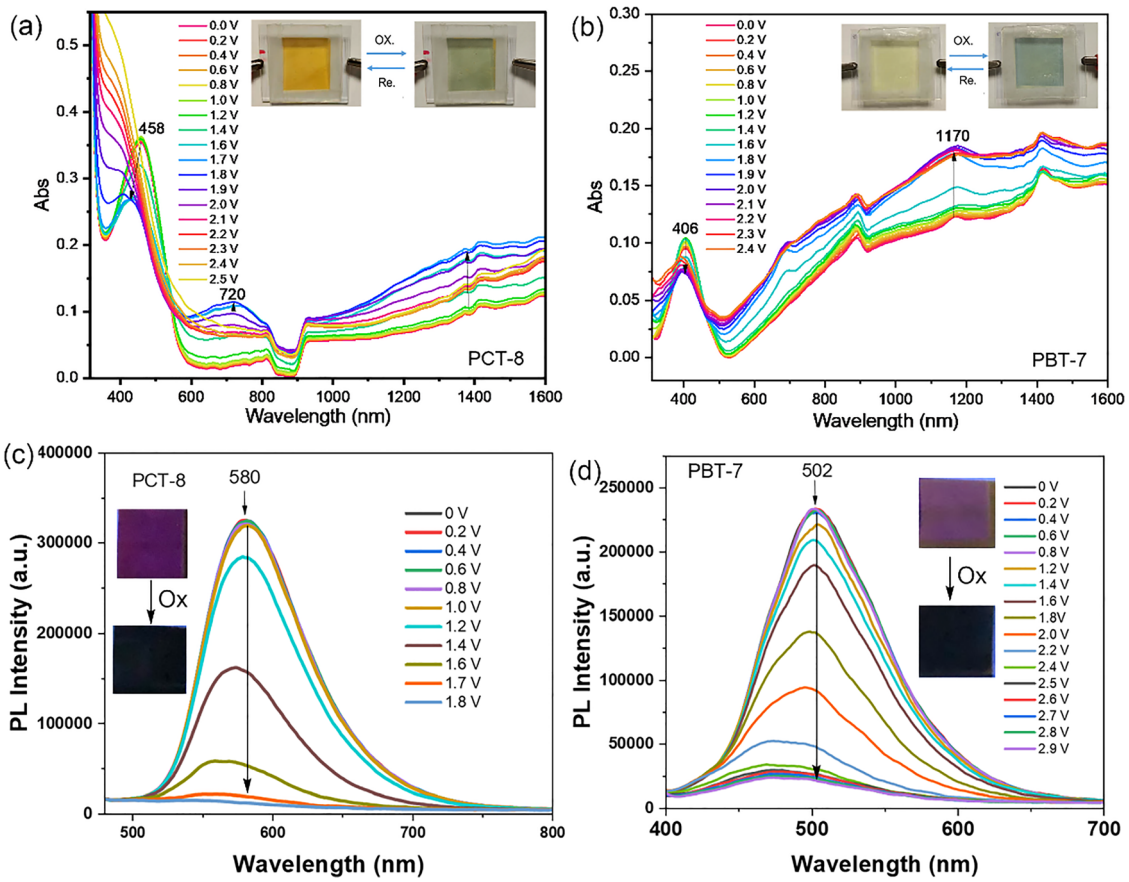

Fig. 4 Electrochromic spectroelectrochemistry of (a) **PCT-8**; (b) **PBT-7**; with inset photographs showing respective colour changes. Electrofluorochromic spectroelectrochemistry of (c) **PCT-8**; (d) **PBT-7**; with inset photographs showing respective fluorescence quenching.

exhibited a switching response time of 25.3 s and an initial optical contrast of 25%. However, this contrast gradually decreased with subsequent cycles (Fig. S7). Further efforts may be required to optimize device fabrication to improve the electrochromic switching performance.

Meanwhile, the electrofluorochromic properties of **PCT-8** and **PBT-7** devices were further investigated under the same device structure (Fig. 4c and d) with photoluminescence (PL) spectra respectively recorded under varying applied voltages. The **PCT-8** and **PBT-7** devices exhibit distinct photoluminescence (PL) peaks at 580 nm and 502 nm, corresponding to pink emission. In both devices, the PL intensity progressively decreases with increasing applied voltage—ranging from 0 to 1.8 V for **PCT-8** and from 0 to +1.8 V for **PBT-7**, indicating voltage-dependent fluorescence quenching, particularly more significantly for **PCT-8**. Applying an electric potential can induce oxidation or reduction of the fluorophore or nearby materials, alter their electronic structures and enhance non-radiative decay pathways, thereby reducing fluorescence. Additionally, charge injection under the electric field can facilitate non-radiative energy transfer from the excited fluorophore to acceptor states or quenchers, further decreasing fluorescence intensity. The trend of voltage-dependent fluorescence quenching suggests that electrochemical doping at elevated voltages suppresses excitonic radiative recombination by increasing charge carrier density and enhancing non-radiative decay. The distinct emission wavelengths further demonstrate the tunable optical properties of these materials, highlighting their potential for optoelectronic applications.

4. Conclusion

This work investigates how specific fused alicyclic rings in electron acceptors influence the optoelectronic properties of conjugated polymers, with a particular focus on the steric hindrance effects of these structures in modulating those properties. By incorporating different alicyclic structures, **PCT-8** and **PBT-7** exhibit distinct absorption behaviors ($\Delta\lambda_{max}$ = 47 nm) and optical band gaps (2.38 eV *vs.* 2.19 eV for **PCT-8** and **PBT-7**), underscoring the critical role of alicyclic rings in tailoring the optical and electronic characteristics of conjugated polymers. Furthermore, both polymers demonstrate voltage-dependent photoluminescence quenching, indicating their dual functionality in electrochromism and fluorescence. This highlights their potential for applications in voltage-tunable color-switching systems and multifunctional optoelectronic devices. This study not only deepens the understanding of how alicyclic ring structures influence the conjugated polymer properties but also provides new insights for designing multifunctional optoelectronic materials.

Author contributions

All authors have read and approved the final manuscript. Their contributions are given below: conceptualization (J. Xu; Z. M. Png); data curation (D. Chen; K. L. Osmund, Chin; J. Xu); funding acquisition (J. Xu); investigation (D. Chen; K. L. Osmund, Chin F. X. Wei); methodology (T. L. Dexter Tam; K. Li); project administration (M. H. Chua); resources (H. Meng; Q. Zhu); supervision (X. Wang; J. Xu); validation (X. Y. Debbie Soo; P. J. Ong); writing – original draft (D. Chen); and writing – review and editing (D. Chen; J. Xu).

Conflicts of interest

The authors declare no competing interests.

Data availability

The data supporting this article have been included as part of the SI. Supplementary information: Synthesis and analytical data of compounds and polymers (TGA, DSC, XRD, AFM, ^{1}HNMR, ^{13}CNMR, mass spectra, and DFT computation). See DOI: https://doi.org/10.1039/d5ma00507h.

CCDC 2450121 (**M4**) and 2450122 (**M5**) contain the supplementary crystallographic data for this paper.[25a,b]

Acknowledgements

This work is financially supported by China Scholarship Council (No. 202306290018, Recipient: Dinghui Chen). The authors would like to acknowledge A*STAR HTCO Fund (grant number: C231218001) for financial support for this work.

References

1 Q. Ye, W. T. Neo, C. M. Cho, S. W. Yang, T. Lin, H. Zhou, H. Yan, X. Lu, C. Chi and J. Xu, *Org. Lett.*, 2014, **16**, 6386–6389.
2 S. Dai, J. Zhou, T.-K. Lau, J. J. Rech, K. Liu, P. Xue, Z. Xie, X. Lu, W. You and X. Zhan, *Small Struct.*, 2020, **1**, 2000006.
3 J.-W. Lee, C. Sun, S.-W. Lee, G.-U. Kim, S. Li, C. Wang, T.-S. Kim, Y.-H. Kim and B. J. Kim, *Energy Environ. Sci.*, 2022, **15**, 4672–4685.
4 S. Yokoyama, S. Utsunomiya, T. Seo, A. Saeki and Y. Ie, *Adv. Sci. (Weinh)*, 2024, **11**, e2405656.
5 B. Russ, A. Glaudell, J. J. Urban, M. L. Chabinyc and R. A. Segalman, *Nat. Rev. Mater.*, 2016, **1**, 1–14.
6 D. Chen, M. H. Chua, Q. He, Q. Zhu, X. Wang, H. Meng, J. Xu and W. Huang, *Chem. Eng. J.*, 2024, 157820, DOI: 10.1016/j.cej.2024.157820.
7 D. Chen, Z. Tong, Q. Rao, X. Liu, H. Meng and W. Huang, *Nat. Commun.*, 2024, **15**, 8457.
8 D. Chen, K. Li, K. L. O. Chin, X. Y. D. Soo, P. J. Ong, Z. M. Png, Q. Zhu, M. H. Chua, X. Wang, H. Meng, W. Huang and J. Xu, *Dyes Pigm.*, 2025, **237**, 112697.
9 D. Chen, X. Zhang, H. Xu, M. Wang, M. Zhu, M. Yang, Q. Zhu, Y. He, Z. Liu, J. Xu and H. Meng, *Macromolecules*, 2024, **57**, 6419–6428.
10 L. Duan, J. Qiao, Y. Sun and Y. Qiu, *Adv. Mater.*, 2011, **23**, 1137–1144.

11 C. M. Cho, Q. Ye, W. T. Neo, T. Lin, X. Lu and J. Xu, *Polym. Chem.*, 2015, **6**, 7570–7579.
12 P. M. Beaujuge, S. Ellinger and J. R. Reynolds, *Nat. Mater.*, 2008, **7**, 795–799.
13 A. D. Todd and C. W. Bielawski, *ACS Macro Lett.*, 2015, **4**, 1254–1258.
14 Y. Guo, W. Li, H. Yu, D. F. Perepichka and H. Meng, *Adv. Energy Mater.*, 2017, **7**, 1601623.
15 A. Dewanji, L. van Dalsen, J. A. Rossi-Ashton, E. Gasson, G. E. M. Crisenza and D. J. Procter, *Nat. Chem.*, 2023, **15**, 43–52.
16 C. M. Amb, P. M. Beaujuge and J. R. Reynolds, *Adv. Mater.*, 2010, **22**, 724–728.
17 X. Lv, W. Li, M. Ouyang, Y. Zhang, D. S. Wright and C. Zhang, *J. Mater. Chem. C*, 2017, **5**, 12–28.
18 H. van Mullekom, *Mater. Sci. Eng.: R*, 2001, **32**, 1–40.
19 K. Mullen and W. Pisula, *J. Am. Chem. Soc.*, 2015, **137**, 9503–9505.
20 W. Li, Y. Guo, Y. Wang, X. Xing, X. Chen, J. Ning, H. Yu, Y. Shi, I. Murtaza and H. Meng, *J. Mater. Chem. A*, 2019, **7**, 116–123.
21 W. H. Tang, L. Ke, L. W. Tan, T. T. Lin, T. Kietzke and Z. K. Chen, *Macromolecules*, 2007, **40**, 6164–6171.
22 Z. Xu, H. Du, M. Yin, B. Wang, J. Zhao and Y. Xie, *Org. Electron.*, 2018, **61**, 1–9.
23 L. Luo, W. Huang, C. Yang, J. Zhang and Q. Zhang, *Front. Phys.*, 2021, **16**, 1–32.
24 D. M. Collard, in *π-Stacked Polymers and Molecules: Theory, Synthesis, and Properties*, ed T. Nakano, Springer Japan, Tokyo, 2014, pp. 185–243, DOI: **10.1007/978-4-431-54129-5_4**.
25 (*a*) D. Chen, K. Le Osmund Chin, X. Y. D. Soo, F. X. Wei, K. Li, P. J. Ong, Q. Zhu, X. Wang, T. L. D. Tam, Z. M. Png, M. H. Chua, H. Meng and J. Xu, CCDC 2450121: Experimental Crystal Structure Determination, 2025, DOI: **10.5517/ccdc.csd.cc2n7k5n**; (*b*) D. Chen, K. Le Osmund Chin, X. Y. D. Soo, F. X. Wei, K. Li, P. J. Ong, Q. Zhu, X. Wang, T. L. D. Tam, Z. M. Png, M. H. Chua, H. Meng and J. Xu, CCDC 2450122: Experimental Crystal Structure Determination, 2025, DOI: **10.5517/ccdc.csd.cc2n7k6p**.